Dynamic Enhancement of B-Mode Cardiac Ultrasound Image Sequences

Ultrasound in Med. & Biol., Vol. ■, No. ■, pp. 1–16, 2017

0301-5629

http://dx.doi.org/10.1016/j.ultrasmedbio.2017.03.006

● *Original Contribution*

DYNAMIC ENHANCEMENT OF B-MODE CARDIAC ULTRASOUND IMAGE SEQUENCES

Antonios Perperidis,* David Cusack,† Audrey White,† Norman McDicken,*
Tom MacGillivray,‡ and Tom Anderson§

*Unit of Medical Physics and Medical Engineering, University of Edinburgh, Edinburgh, UK; †Echocardiography Department, Western General Hospital, NHS Scotland, Edinburgh, UK; ‡Clinical Research Imaging Centre, University of Edinburgh, Edinburgh, UK; and §Centre for Cardiovascular Science, University of Edinburgh, Edinburgh, UK

(*Received* 20 *October* 2016; *revised* 6 *February* 2017; *in final form* 16 *March* 2017)

Abstract—Limited contrast, along with speckle and acoustic noise, can reduce the diagnostic value of echocardiographic images. This study introduces dynamic histogram-based intensity mapping (DHBIM), a novel approach employing temporal variations in the cumulative histograms of cardiac ultrasound images to contrast enhance the imaged structures. DHBIM is then combined with spatial compounding to compensate for noise and speckle. The proposed techniques are quantitatively assessed (32 clinical data sets) employing (i) standard image quality measures and (ii) the repeatability of routine clinical measurements, such as chamber diameter and wall thickness. DHBIM introduces a mean increase of 120.9% in tissue/chamber detectability, improving the overall repeatability of clinical measurements by 17%. The integrated approach of DHBIM followed by spatial compounding provides the best overall enhancement of image quality and diagnostic value, consistently outperforming the individual approaches and achieving a 401.4% average increase in tissue/chamber detectability with an associated 24.3% improvement in the overall repeatability of clinical measurements. (E-mail: A.Perperidis@hw.ac.uk) © **2017 The Authors. Published by Elsevier Inc. on behalf of World Federation for Ultrasound in Medicine & Biology. This is an open access article under the CC BY license (http://creativecommons.org/licenses/by/4.0/).**

Key Words: **Ultrasound, Echocardiography, Histogram processing, Image enhancement, Contrast enhancement, Noise suppression.**

INTRODUCTION

Transthoracic echocardiography, although a valuable tool for the assessment of cardiac morphology and function, suffers from a range of artifacts because of the interaction of the transmitted ultrasound with structures such as bone, lung and fat. These interactions may cause acoustical noise and speckle, reduce contrast and limit the delineation of fine anatomic detail. Such artifacts may therefore limit the (i) diagnostic value and (ii) effectiveness of post-processing tools on cardiac ultrasound images. Although advances in data acquisition technologies have substantially improved cardiac ultrasound data, a systematic study performed at the Echocardiography Department of the Western General Hospital (Edinburgh, Scotland) indicated that a considerable (≤30%) portion of routine cardiac scans generate low-quality images of limited diagnostic value (corrupted structures, limiting or even prohibiting clinical measurements). The results have been used for educational purposes within the department and have not been published yet. Consequently, there is research interest in the development of post-processing methods that address these limitations, enhancing the image quality and diagnostic value of cardiac ultrasound.

Numerous approaches to enhancement of cardiac ultrasound images have been suggested (Perperidis 2016). Spatial compounding is a popular method that suppresses noise by combining partially decorrelated images produced by imaging the target region of interest from different viewing angles. Tissue structures present in all the partially decorrelated views are enhanced, whereas artifacts not present in all views are suppressed. There are studies that have employed spatial compounding through transducer repositioning for the enhancement of 3-D cardiac ultrasound data (Gooding et al. 2010;

Address correspondence to: Antonios Perperidis, Institute of Signals Sensors and Systems, School of Engineering and Physical Sciences, Heriot-Watt University, Edinburgh, EH14 4 AS, UK. E-mail: A.Perperidis@hw.ac.uk

Mulder et al. 2014; Rajpoot et al. 2011; Szmigielski et al. 2010; Yao et al. 2010). Some studies have attempted to enhance 2-D cardiac ultrasound images by averaging temporally consecutive frames (Achmad et al. 2009; dos Reis et al. 2009; Li et al. 1994; Petrovic et al. 1986). Other studies have utilised the repeated rhythmic contractions of the heart to acquire and compound multiple partially decorrelated 2-D images of the same cardiac phase over consecutive cardiac cycles through a single acoustic window. The process has been referred to as *temporal compounding* (Abiko et al. 1997; Amorim et al. 2009; Klingler et al. 1989; Olstad 2002; Perperidis et al. 2009; Rigney and Wei 1988; Unser et al. 1989; van Ocken et al. 1981; Vitale et al. 1993).

Although spatial compounding is primarily a tool for noise and speckle suppression, it has also been found to compensate for other artefacts in cardiac ultrasound, including partial shadowing and reverberations. However, spatial compounding has no noteworthy effect in enhancing the cardiac tissue/chamber contrast. Limited contrast between cardiac tissue and chambers constitutes a major limitation in cardiac ultrasound images, potentially making (when combined with noise) the delineation of cardiac structures very challenging. Non-contrast tissue harmonic imaging (THI) is a well-established approach (sometimes employed as the standard acquisition mode) for enhancing the contrast and delineation between cardiac tissue and chambers (Averkiou et al. 1997; Becher et al. 1998; Caidahl et al. 1998; Franke et al. 2000; Ward et al. 1997). However, challenging cases still arise where effective post-processing techniques for the contrast enhancement between cardiac tissue and chambers could be beneficial. A number of filters (Finn et al. 2011; Tay et al. 2010; Yue et al. 2005; Zong et al. 1998) and spatial compounding approaches (Rajpoot et al. 2009; Szmigielski et al. 2010; Yao and Penney 2008) have been claimed to enhance the structure boundaries along with the contrast between cardiac tissue and chambers. However, many of these noise suppression methods actually perform contrast and boundary preservation rather than enhancement. Consequently, dedicated methods that suppress noise in cardiac chambers while enhancing the contrast and detectability between cardiac tissue and chamber structures are desirable.

To distinguish and enhance the contrast between tissue and chamber pixels, a method to derive an effective tissue/chamber threshold is required. Sezgin and Sankur (2004) categorised thresholding methods into six groups: (i) histogram shape, (ii) clustering, (iii) entropy, (iv) image attributes, (v) spatial information and (vi) local characteristics. Histogram-based methods are very popular because of their simplicity and efficiency. Therefore, the multiframe nature of cardiac ultrasound data (exceeding 100 frames/s on state-of-the-art scanners) makes histogram based thresholding very appealing.

Abdullah-Al-Wadud et al. (2007) and Ibrahim and Kong (2007) introduced contrast enhancement techniques that analyse the shape of the histogram and partition it based on local minima and maxima, respectively. They both then assigned specific gray-level ranges to each partition before performing histogram equalisation on them individually. Both techniques performed well in low-contrast images. However, the high levels of noise along with speckle and the subsequently more complex histograms in cardiac ultrasound data impose a severe limitation on the potential of similar histogram shape-based techniques (Hammoude 1998). Zwirn and Akselrod (2004, 2005) introduced the adaptive brightness transfer function (ABTF) based on the assumption that the histogram of cardiac ultrasound images can be approximated by the sum of three overlapping Gaussian distributions. The intersections between these three Gaussians would act as thresholds, with each section of the histogram being individually processed using a number of techniques, including histogram equalisation, specification and scaling. The results presented on suppressing chamber noise and enhancing contrast between cardiac tissue and chambers were promising. However, like most histogram shape-based approaches, ABTF makes a strong assumption about the shape of the histograms of the processed images. Although some images may conform to this paradigm, such an assumption may result in considerable pixel misclassification, especially in cases of large overlap between the fitted Gaussians. Moreover, ABTF assumed constant illumination throughout the field of view, which in many scans is not the case because of suboptimal manual setting of the time gain compensation (TGC).

The aim of this study was to introduce a cardiac ultrasound image enhancement approach that suppresses noise and speckle while increasing contrast and detectability between cardiac tissue and chambers. Initially, dynamic histogram based intensity mapping (DHBIM) is introduced as a novel, simple and efficient method for suppressing cardiac chamber noise, enhancing tissue speckle and increasing tissue/chamber detectability. Unlike previous approaches, DHBIM employs variations over time in the cumulative histograms of cardiac ultrasound image sequences to derive a tissue/chamber threshold, avoiding strong assumptions on histogram shape. DHBIM is then combined with a temporal compounding (Perperidis et al. 2015) approach that also makes use of image variations over time to compensate for noise and speckle, as well as other artefacts that may momentarily appear, such as shadowing and reverberations. The results of the individual (DHBIM and temporal compounding) approaches as well as the integrated approach are finally compared.

METHODS

Data acquisition and classification

Cardiac data from 32 patients were acquired according to the standards adopted by the British Society of Echocardiography (Feigenbaum et al. 2005; Henry et al. 1980; Wharton et al. 2012) at the Western General Hospital, Edinburgh. All data sets used in this study were selected from fully anonymised cine loops recorded during routine clinical examinations in the course of normal care with no intention to use them in research at the time of collection. Consequently, no National Health Service (NHS) ethics approval was required under the terms of the *Governance Arrangements for Research Ethics Committees: A Harmonised Edition* (Department of Health Research and Development Directorate of England et al. 2011). The data sets were representative of patients examined in the department and so included data over the full diagnostic quality range of high (12), average (12) or low (8) (as specified by an experienced echocardiographer). B-Mode data of at least 25 cardiac cycles of the parasternal long-axis (PLAX) view were selected with no other quality-related selection criteria being used. The PLAX view was utilised because it is common in clinical practice and enables (i) the visualisation of multiple cardiac structures and (ii) the acquisition of a range of clinical measurements that are essential during the diagnostic process. All data were acquired using a GE Vivid 7 Dimension ultrasound scanner (GE Healthcare, Little Chalfont, UK) along with a 3-MHz phased array probe employing tissue harmonic imaging as standard acquisition mode. Images were captured at 25 frames/s (fps). Other acquisition parameters such as acquisition depth, focus depth, sector width, gain and TGC were manually optimised for each subject. Finally, B-mode image sequences of 434 × 636 pixels were exported in DICOM format with no compression applied.

Data analysis: Contrast enhancement

Dynamic histogram-based intensity mapping was implemented using a three-step process (Fig. 1a): (i) identification and compression of any underutilised intensity levels within the frame sequence, (ii) derivation of a cardiac tissue/chamber intensity threshold and (iii) enhancement of the contrast between cardiac tissue and chamber structures.

A B-mode cardiac cycle can be described by an ordered sequence of n 2-D images $S(x,y)$ with a fixed field of view Ω_S and an acquisition time t in the temporal direction. The resulting image sequence can be viewed as 2-D + time structure $S(x,y,t)$ defined on the spatiotemporal domain $\Omega_S \times [t_1, t_n]$. The goal was therefore to derive an intensity transformation function T of the form:

$$T : S(x, y, t) \rightarrow S'(x, y, t) \quad [1]$$

where $S(x,y,t)$ represented the gray level of the original image at point (x,y) and time $t \in [1, M]$, and $S'(x,y,t)$ represented the corresponding gray level on the processed data of image. Transformation T mapped the intensity level $S(x,y,t)$ at any point in an image sequence into a corresponding intensity level $S'(x,y,t)$. Any parameters required to define the intensity transfer function T (intensity mapping) were automatically derived by analysing the dynamic variations in the image histograms through a sequence of consecutive cardiac ultrasound frames. The normalized histogram of a digital image with gray levels in the range [0,N] ($N = 255$) was a discrete function (Gonzalez and Woods 2001)

$$p(r_k) = n_k / n \quad [2]$$

where r_k is the kth gray level, n_k is the number of pixels in the image having gray level r_k for $k \in [0, N]$ and n denotes the total number of pixels in the image (*i.e.*, $p(r_k)$ denotes the probability of occurrence of gray level r_k).

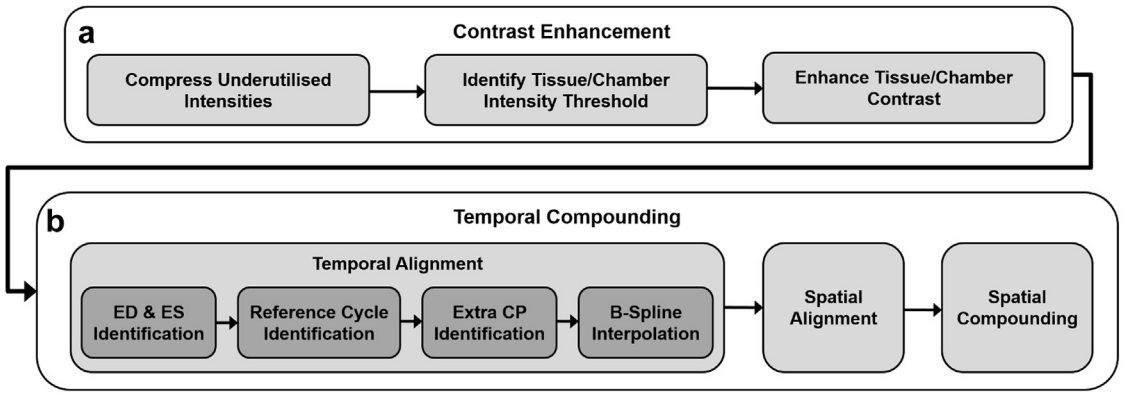

Fig. 1. Block diagram of (a) the proposed dynamic, contrast enhancement approach followed by (b) temporal compounding to a holistic image enhancement methodology.

Identification and compression of underutilised intensities within the frame sequence

Underutilised intensity levels can be defined as intensity levels that either are not utilised because of limited imaging dynamic range or correspond to regions that are not affected by the constant motion of the cardiac walls (such as central regions of chambers). Underutilised intensity levels within the B-mode frame sequences were identified by analysing the dynamic temporal variations in the image histograms corresponding to a sequence of consecutive cardiac ultrasound frames. A normalised histogram was generated for each frame in the B-mode sequence:

$$p(r_k,t) = n_k(t)/n \quad [3]$$

The standard deviation (SD) of the variations in each intensity level over consecutive frames was then derived:

$$\sigma_p(r_k) = \sqrt{\frac{1}{M}\sum_{t=1}^{M}\left(p(r_k,t)-\mu\right)^2} \quad [4]$$

where M is the total number of frames, and μ is the mean $p\,(r_k)$ value across the B-mode frame sequence. A heuristic threshold set as $<1\%$ of the maximum value observed over the derived $\sigma_p\,(r_k)$ profile was utilised to identify such underutilised intensity levels:

$$\begin{aligned} th_l &= \left\{\max(i), i\in[1,N] : \left[\sigma_p(r_0),\sigma_p(r_i)\right] < 0.01\times \max_k \sigma(r_k)\right\} \\ th_u &= \left\{\min(j),\ j\in[1,N] : \left[\sigma_p(r_j),\sigma_p(r_N)\right] < 0.01\times \max_k \sigma(r_k)\right\} \end{aligned} \quad [5]$$

where th_l and th_u are the estimated lower and upper thresholds, respectively. Subsequently, a simple piecewise-linear transformation T_1 function was used as an intensity mapping between the original and the processed frame sequences

$$T_1(r_k) = \begin{cases} 0, & \text{if } k \le th_l \\ N, & \text{if } k \ge th_u \\ (a\times r_k)+b, & \text{if } th_l < k < th_u \end{cases} \quad [6]$$

where r_k is the kth intensity level, $a=N/(th_u-th_l)$ and $b=(N\times th_l)/(th_u-th_l)$ represents the slope and y-intercept of the linear contrast stretching, respectively. T_1 compressed all intensity levels below or equal to th_l to 0 (black-level expansion) and all intensity levels above or equal to th_u to $N = 255$ (white-level expansion), increasing the dynamic range of the imaged cardiac structure.

Identification of tissue/chamber intensity threshold

The novel approach proposed in this study was based on some basic observations in cardiac ultrasound images. More precisely, the cardiac tissue/chamber intensity threshold th_{ct}, was identified by analysing the dynamic variations in the image histograms over a sequence of consecutive cardiac ultrasound frames. Let $n_c\,(t_d)$ and $n_c\,(t_s)$ represent the true number of cardiac chamber pixels within an end-diastole (ED) (t_d) and an end-systole (ES) (t_s) frame, respectively (corresponding to a correct tissue/chamber threshold th_{ct}), and $DS_c = n_c\,(t_d) - n_c\,(t_s)$ represent the difference in the number of chamber pixels between ED (where ventricular chambers reach maximum volume) and ES (where ventricular chambers reach minimum volume). Because $th_r \in [0, N]$ represents an arbitrarily selected tissue/chamber gray-level threshold, there are three possible cases.

In the first case, $th_r < th_{ct}$; therefore,

$$\begin{aligned} DS_r &= n_r(t_d) - n_r(t_s) = \left(n_c(t_d) - n_{ft}(t_d)\right) - \left(n_c(t_s) - n_{ft}(t_s)\right) \\ &= \left(n_c(t_d) - n_c(t_s)\right) - \left(n_{ft}(t_d) - n_{ft}(t_s)\right) \\ &= DS_c - \left(n_{ft}(t_d) - n_{ft}(t_s)\right) \end{aligned} \quad [7]$$

where $n_r\,(t_d)$ and $n_r\,(t_s)$ are the total number of pixels identified as chamber pixels (*i.e.,* pixels with intensity less than threshold th_r), and $n_{ft}\,(t_d)$ and $n_{ft}\,(t_s)$ are the number of chamber pixels falsely identified as tissue pixels in the ED and ES frames, respectively. Because the number of chamber pixels reaches its maximum in ED and its minimum in ES, it is expected that $(n_{ft}(t_d) - n_{ft}(t_s)) > 0$ and, therefore, $DS_r < DS_c$.

In the second case, $th_r > th_{ct}$; therefore,

$$\begin{aligned} DS_r &= n_r(t_d) - n_r(t_s) = \left(n_c(t_d) + n_{fc}(t_d)\right) - \left(n_c(t_s) + n_{fc}(t_s)\right) \\ &= \left(n_c(t_d) - n_c(t_s)\right) + \left(n_{fc}(t_d) - n_{fc}(t_s)\right) \\ &= DS_c + \left(n_{fc}(t_d) - n_{fc}(t_s)\right) \end{aligned} \quad [8]$$

where $n_{fc}(t_d)$ and $n_{fc}(t_d)$ are the number of tissue pixels falsely identified as chamber pixels in the ED and ES frames, respectively. Given that the number of tissue pixels reaches its minimum in ED and its maximum in ES, it is expected that $(n_{fc}(t_d) - n_{fc}(t_s)) < 0$, and therefore,

$DS_r < DS_c$. Consequently, in the third and last case, where $th_r = th_{ct}$, $\mathrm{DS_r}$ is expected to attain its maximum value, which is equal to DS_c.

In this study, the number of pixels identified as "chamber" n_r for a given threshold th_r (pixel intensities less than threshold th_r) was derived over the full range of possible threshold values (*i.e.*, $th_r \in [0, N]$, $N = 255$) utilising the cumulative image histogram

$$n_{r_k} = cH(r_k) = \sum_{i=0}^{k} n_i \qquad [9]$$

where r_k is the kth gray level, and n_i is the number of pixels in the image having gray level i. Considering the high noise level along with other artifacts (such as shadowing) present in cardiac ultrasound data, a more robust measure of determining the variation in the number of chamber pixels between ED and ES (compared with DS_r) was required. As a result, the standard deviation (SD) of the population variations over consecutive frames for each intensity level within the cumulative histogram was utilised:

$$\sigma_n(r_k) = \sqrt{\frac{1}{M}\sum_{t=1}^{M}\left(n_{r_k}(t) - \mu\right)^2}. \qquad [10]$$

Here M is the total number of frames, and μ is the mean n_{r_k} value over the B-mode frame sequence. Similar to DS_r, the SD was expected to have a maximum value for th_r equal to the actual tissue/chamber threshold ($th_r = th_{ct}$):

$$th_{ct} = k : \max_{k \in [0,N]} \left(\sigma_n(r_k)\right). \qquad [11]$$

To further enhance the robustness of the approach, making it less susceptible to outliers, data from multiple ED–ES sequences were utilised during the derivation and allocation of the maximum SD value.

Enhance contrast between cardiac tissue and chamber structures

Having identified threshold th_{ct} defining the intensity levels corresponding to cardiac chamber and tissue, a piecewise-linear transformation function (intensity mapping) was employed to (i) suppress noise in cardiac chambers; (ii) increase the displayed dynamic range in cardiac tissue, enhancing the available tissue speckle information; and (iii) enhance the contrast between cardiac tissue and chamber. The shape of the transformation T_2 was controlled by threshold th_{ct} and was defined as

$$T_2(r_k) = \begin{cases} r_k/2, & \text{if } k \le th_{ct} \\ \alpha * r_k + \beta, & \text{if } k > th_{ct} \end{cases} \qquad [12]$$

where r_k is the kth intensity level, α represents the slope of the linear contrast stretching $\left(\alpha = 1 + \frac{th_{ct}}{2*(N-th_{ct})}\right)$ and β represents its y-intercept $\left(\beta = -N\frac{N*th_{ct}}{2*(N-th_{ct})}\right)$.

Subsectioning

From experience, the level of chamber noise as well as the tissue/chamber contrast can vary considerably across the imaged field of view. Such variations can be attributed to the complex interaction of each structure with the transmitted ultrasound signals, as well as non-optimal TGC settings during data acquisition. To compensate for such potential variations, each step was performed on a number of non-overlapping subsectors along the y-axis of the cardiac scan (Fig. 2). Each non-overlapping sector would act as a binary mask, with no information outside the sector being used throughout the tissue/chamber threshold estimation process. A prerequisite for each subsector was that it contain both cardiac tissue and chamber structures so that temporal histogram variations could generate a representative tissue/chamber threshold. Identifying a suitable number of subsectors was essential for the effectiveness and efficiency of the DHBIM process. The sectors were therefore empirically selected to include different cardiac sections imaged in a parasternal long-axis cardiac ultrasound scan. A linear interpolation between the individual extracted thresholds was employed across the boundaries of each sector to avoid any intensity level discontinuities.

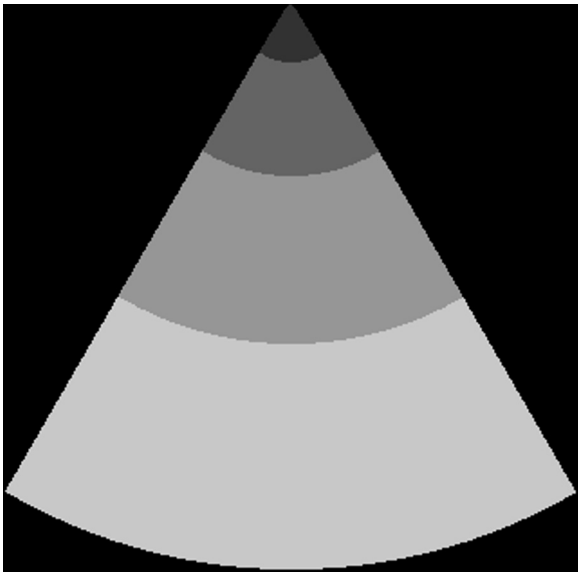

Fig. 2. Partition of scan in four non-overlapping subsectors along the y-axis.

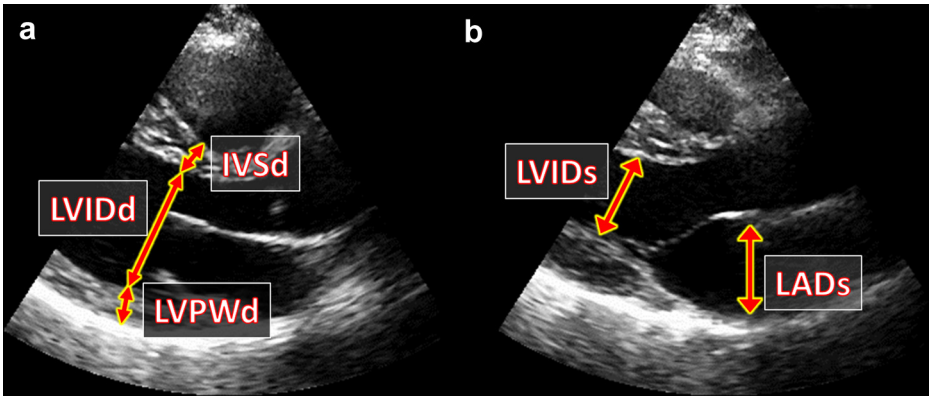

Fig. 3. (a) Example measurements of the interventricular septum thickness (IVSd), left ventricular internal dimension (LVIDd) and left ventricular posterior wall (LVPWd) during end diastole (ED). (b) Example measurements of left ventricular internal dimension (LVIDs) and left atrial dimension (LADs) during end systole (ES). All measurements were made across the parasternal long-axis view of the heart.

Data analysis: Noise suppression

To further enhance the image quality and diagnostic value of the imaged cardiac structures, temporal compounding was employed as a noise/speckle suppression technique. Temporal compounding was implemented using a three-step process (Fig. 1b), including (i) temporal alignment of the multicycle data to a reference cardiac cycle, (ii) spatial alignment of the temporally aligned frames and (iii) spatial compounding of the spatiotemporally aligned data. Detailed information can be found in Perperidis et al. (2015).

Step 1: Temporal alignment. The temporal alignment process was further divided into four steps.

Identification of ED and ES frames. All ED and ES frames within a multicycle data set were identified utilising intensity information (a robust adaptation of normalised cross-correlation [NXC]) from the B-mode image sequence. The method was based on the periodic ventricular deformation during the cardiac cycle and required the manual identification of only one ED (ED1) and one ES (ES1) frame. The remaining end-diastolic frames within the B-mode sequence were automatically identified demonstrating maximum similarity with ED1 and minimum similarity to ES1. Similarly, the remaining end-systolic frames were automatically identified demonstrating maximum similarity with ES1 and minimum similarity to ED1.

Selection of a representative reference cardiac cycle. For each cardiac cycle, a weighting factor was defined comprising the difference (in number of frames) of the current diastole and systole lengths from the mean diastole and systole lengths over the whole

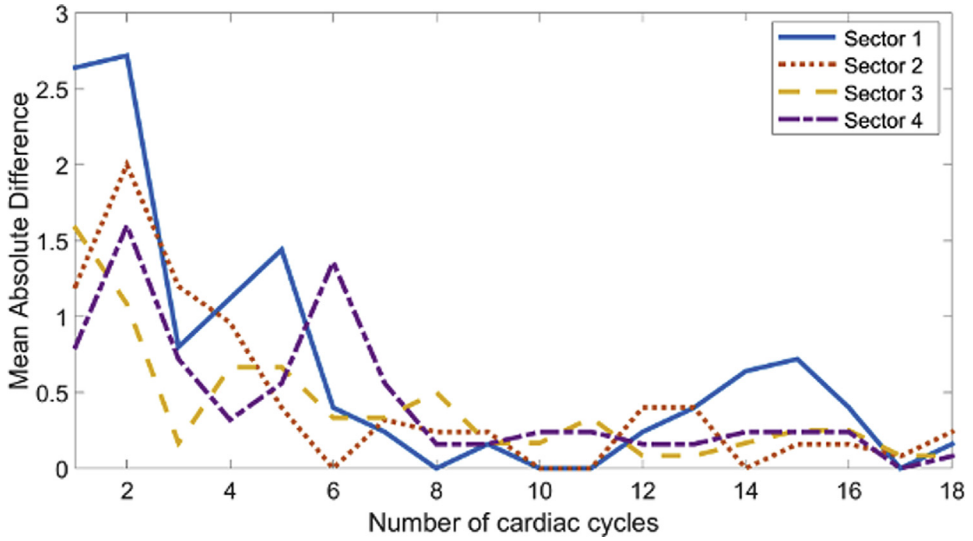

Fig. 4. Mean absolute difference (MAD) in threshold estimation for increasing number of cardiac cycles. Separate curves for each of the four non-overlapping regions are provided.

multicycle data set. The cardiac cycle with the lowest weighting factor was considered the most representative within the data set and was therefore selected as the reference cardiac cycle for all remaining cardiac cycles to be temporally and spatially registered to.

Identification of additional control points. To provide a reliable representation of the seven independent stages of a cardiac cycle (Berne et al. 2004; Bray et al. 1999; Guyton 1991; Guyton and Hall 1997), two additional frames were introduced at regular temporal intervals in each of the contraction and relaxation phases of the reference cycle (*i.e.,* 7 points in total). Image similarity (NXC) was then employed to identify equivalent frames within the remaining cardiac cycles. These frames would act as additional control points during the interpolation process, generating an alignment independent of the nature of the temporal variations throughout the multicycle data.

Interpolation process. The final stage of the temporal alignment between two frame sequences established a correspondence between frames in the reference and the aligned cardiac cycles. Both global and local temporal variations were addressed by applying a 1-D interpolating cubic B-spline curve (Barsky 1982; Caglar et al. 2006) between the reference and all the remaining cardiac cycles within a multicycle frame sequence.

Step 2: Spatial alignment. A rigid body transformation was found to correct for most of the spatial misalignments observed throughout the multicycle data sets (mostly caused by respiratory motion). More precisely, Nelder and Mead (1965) simplex approach was employed to derive the optimal transformation that maximised the similarity (NXC) between the registered images.

Step 3: Spatial compounding. Each frame within the reference cardiac cycle was replaced by a compound frame generated by averaging the 12 most similar spatiotemporally aligned frames, one from each cardiac cycle. Intensity averaging was employed as a well-established and effective compounding method for noise/speckle suppression in ultrasound data sets. Dissimilar frames (potentially caused by spatiotemporal misalignments) were automatically identified, employing a threshold on their image similarity with the reference frame, and discarded before spatial compounding to minimise the tissue/chamber boundary blurring being introduced on the compound images.

Table 2. Range of total number of underutilised intensity levels within the 32 cardiac ultrasound data sets

	Underutilised level
Minimum	0
Maximum	146
Mean	28
Standard deviation	34

Clinical assessment

An experienced echocardiographer assessed the effect of proposed image enhancement approaches on the diagnostic value of cardiac ultrasound images. Quantitative assessment was achieved by performing routine clinical measurements on ED and ES frames from both the original unprocessed and the processed data. More precisely, a sequence of ED frames was presented, and (i) interventricular septal thickness (IVSd), (ii) left ventricular internal dimension (LVIDd) and (iii) left ventricular posterior wall (LVPWd) measurements were performed on each frame (Fig. 3). Similarly, a sequence of ES frames was presented, and (i) left ventricular internal dimension (LVIDs) and (ii) left atrium dimension (LADs) measurements were performed on each frame (Fig. 3). The selected measurements are widely used during routine clinical cardiac ultrasound examinations and provide valuable information on the state and function of the examined heart. More information is available in Feigenbaum et al. (2005). Each frame sequence contained one original and three enhanced frames (compounded, contrast enhanced and combination) for each of the data sets (128 frames in total). The order of the frames was randomised to ensure no bias in the results. All clinical measurements were performed twice, according to the standards adopted by the British Society of Echocardiography (Feigenbaum et al. 2005; Fuster et al. 2008; Henry et al. 1980; Wharton et al. 2012), to enable the examination of measurement repeatability and agreement among the techniques (Bland and Altman 1986).

Table 1. Numbers and percentages of 32 cardiac ultrasound data sets exhibiting underutilised gray levels within the image intensity range

Sector	No. of data sets with $th_l>0$	No. of data sets with $th_u<255$	No. of data sets with underutilised intensities
1	14 (43.8%)	7 (21.9%)	18 (56.3%)
2	22 (68.8%)	6 (18.8%)	26 (81.3%)
3	9 (28.1%)	19 (59.4%)	25 (78.1%)
4	5 (15.6%)	11 (34.4%)	13 (40.6%)
Total	50 (39.1%)	43 (33.6%)	82 (64.1%)

Table 3. Comparison of the effects of individual and integrated methods on image quality metrics

	Temporally compounded	Contrast enhanced	Contrast enhanced and temporally compounded
Tissue SNR	87.1% (63.0%)*	−37.0% (15.9%)	14.1% (38.3%)
Chamber SNR	143.1% (75.0%)	−26.8% (17.4%)	78.2% (59.7%)
Contrast	−3.1% (16.4%)	73.8% (48.1%)	72.1% (56.4%)
SDNR	128.6% (85.1%)	120.9% (52.3%)	401.4% (182.3%)

SDNR = signal difference-to-noise ratio; SNR = signal-to-noise ratio.
* Mean (standard deviation).

RESULTS

To ensure that an accurate and robust tissue/chamber threshold was derived, images from multiple cardiac cycles were utilised. More precisely, the mean absolute difference (MAD) of the derived threshold th_{ct} for increasing number cardiac cycles was estimated as

$$MAD(t) = \frac{1}{K}\sum_{k=1}^{K}\sqrt{\left(th_{ct}^{k}(t) - th_{ct}^{k}(t-1)\right)^{2}} \qquad [13]$$

with $K = 32$ being the number of examined data sets and t being the number of cardiac cycles employed in the threshold th_{ct} estimation of the kth data set. Figure 4 illustrates the MAD for increasing number of cardiac cycles for each of the four non-overlapping subsectors. In all subsectors, the threshold estimation converges (MAD <0.5) within eight cardiac cycles. Sector 1 at the top of the field of view exhibits (because of its small size) the most variate behavior in the threshold estimation over series of eight or more cardiac cycles. Twelve cardiac cycles have previously been reported to provide a good trade-off between image enhancement and acquisition and processing requirements in temporal compounding (Perperidis et al. 2015). Although fewer cardiac cycles (*e.g.,* 8 cycles) would suffice when 12 cardiac cycles cannot be obtained, images from 12 cardiac cycles were used in the estimation of the results presented in the remainder of this study.

Each step of the algorithm was performed on a number of non-overlapping subsectors along the y-axis of each cardiac scan. A prerequisite for each subsector was that it contain both cardiac tissue and chamber structures so that temporal histogram variations could generate a representative tissue/chamber threshold. After thorough examination, it was empirically estimated that four subsectors (Fig. 2) were the most computationally efficient option (smallest number of subsectors) that provided a fair representation of the (i) near-field noise, (ii) right ventricle (RV) chamber, (iii) left ventricle (LV) chamber and (iv) left atrium (LA) chamber.

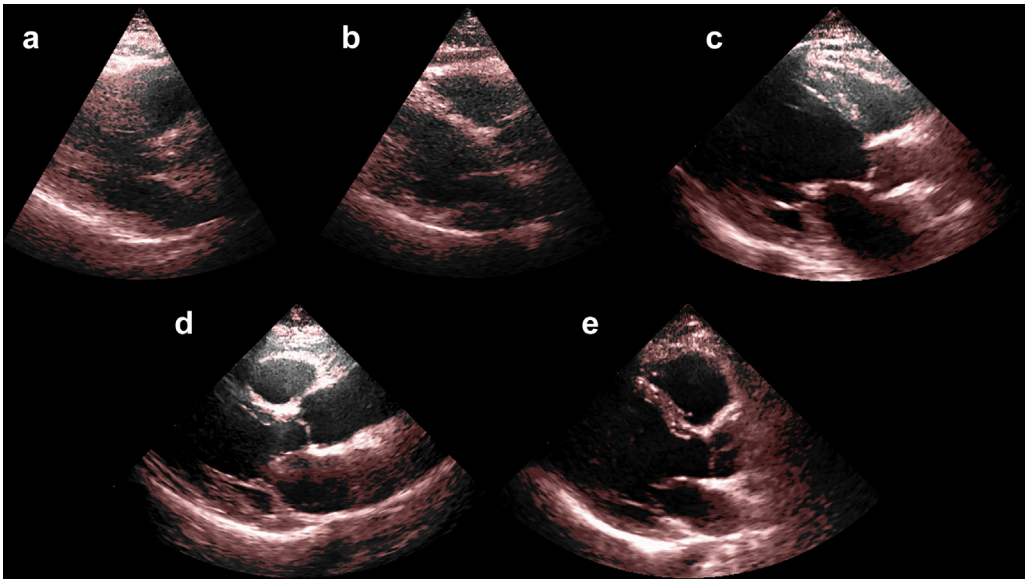

Fig. 5. Binary masks overlaid on top of B-mode end-diastole frames of (a,b) low, (c,d) average and (e) high diagnostic value.

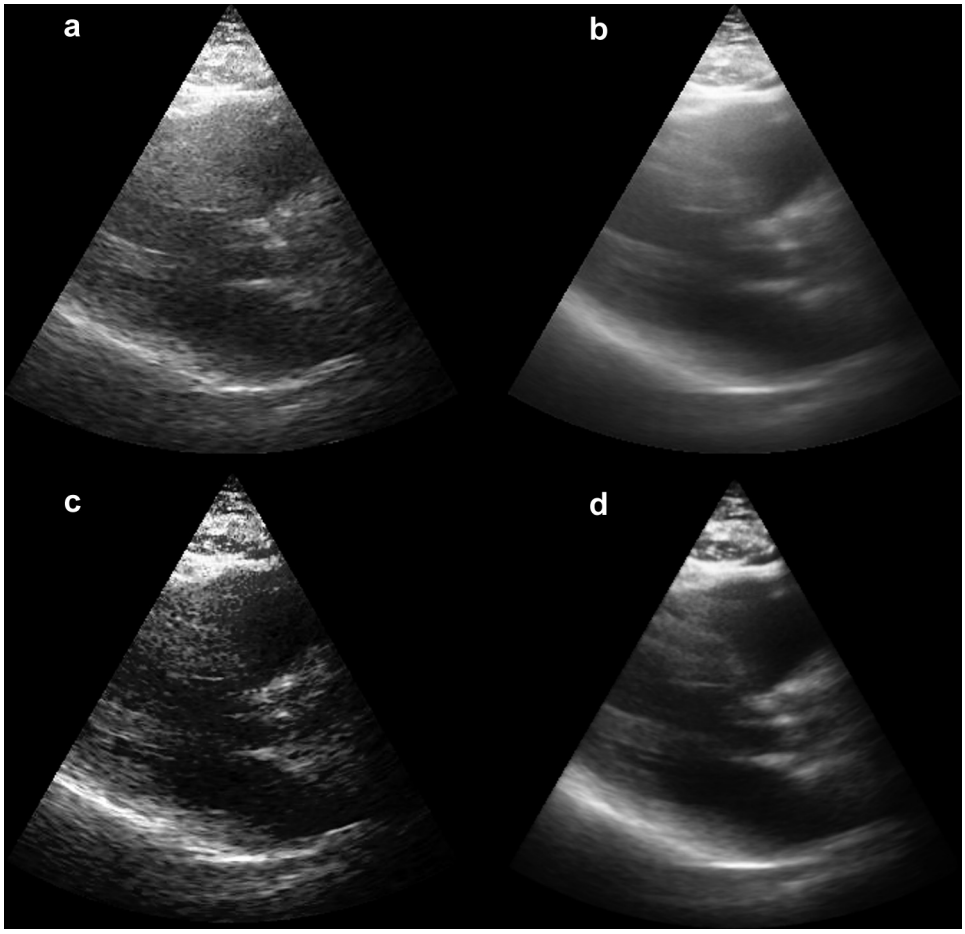

Fig. 6. Images characterised as of very low diagnostic value. (a) Original, (b) compounded, (c) contrast-enhanced and (d) combined end-diastole frames.

Underutilised intensities

Table 1 enumerates the data sets identified as having underutilised gray levels within the image intensity range. The threshold identification algorithm was independently executed in four non-overlapping subsectors of each cardiac scan. Table 2 provides the range of the total number of underutilised intensity levels within the 32 cardiac ultrasound data sets.

Effect on SNR, contrast and SDNR

Two 11 × 11-pixel regions of interest (ROIs) corresponding to the IVS and the RV chamber were manually defined on each of the 32 patient data sets. The pixel intensity values within each ROI were used to estimate the tissue and chamber signal-to-noise ratio $(SNR = \mu/\sigma)$, where μ and σ refer to the mean and standard deviation of the corresponding ROI intensity values. In a similar manner, the tissue/chamber contrast $\left(C = \frac{|\mu_T - \mu_C|}{(\mu_T + \mu_C)/2}\right)$ and signal difference-to-noise ratio $\left(\mathrm{SDNR} = \frac{|\mu_T - \mu_C|}{\sigma_C}\right)$, also referred to as the detectability index, were derived, where μ_T and μ_c corresponded to the mean tissue and chamber intensity levels, respectively, and σ_c corresponds to the chamber standard deviation. Table 3 summarises and provides a direct comparison of the mean effects of the individual and integrated image enhancement methods on all four image quality metrics.

Visual effect

Figure 5 illustrates characteristic examples of the binary masks distinguishing between cardiac tissue and chambers over a range of image qualities. Figures 6 to 10 display five example ED frames before and after three image enhancement methods (compounding, contrast enhancement, combination) are applied to their corresponding multicycle data sets. Data sets covering a range of image and diagnostic qualities (2 low, 2 average and 1 high) were selected to best illustrate the effect of each enhancement approach on cardiac ultrasound data.

Effect on diagnostic value

Bland–Altman analysis (Bland and Altman 1986) was employed for the quantitative assessment of the

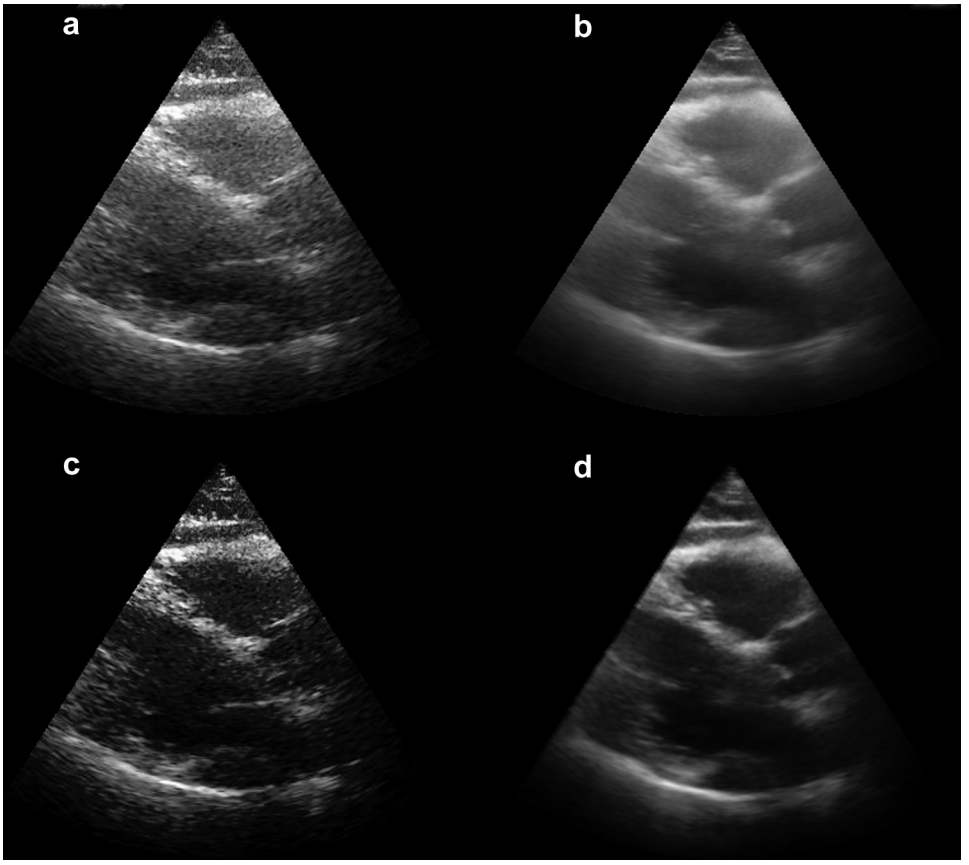

Fig. 7. Images characterised as of low diagnostic value. (a) Original, (b) compounded, (c) contrast-enhanced and (d) combined end-diastole frames.

effect of each enhancement approach on routine clinical measurements. The Bland–Altman analysis derives the coefficient of repeatability (CR) denoting (i) the level of repeatability of clinical measurements performed using a single approach, and (ii) the level of agreement between corresponding measurements performed using different approaches. In all cases, the lower the CR, the higher are the measurement repeatability and agreement. Moreover, the mean difference indicates the presence of any bias in the corresponding measurements. Table 4 summarises the bias and repeatability level coefficients derived from the individual plots for each clinical measurement. Similarly, Table 5 summarises the bias and agreement of each clinical measurement when performed on enhanced images, compared with measurements on the original, unprocessed data.

DISCUSSION

In this study, tissue/chamber contrast enhancement was applied to the original B-mode data before spatial compounding. Inverting the process is expected to generate a similar effect on cardiac ultrasound data. However, spatial compounding can sometimes introduce minor tissue/chamber boundary blurring, which in turn can have a limiting effect on the derivation of an effective threshold. Furthermore, the effectiveness of compounding is heavily based on the accurate alignment of the multicycle data. Suppressing chamber noise and enhancing tissue/chamber contrast before spatial compounding can therefore increase the accuracy of the spatiotemporal data registration, resulting in more effective image enhancement.

Identify underutilised intensities

Table 1 indicates that 64.1% of the data sets included underutilised intensity levels spread fairly evenly in the lower (33.6%) and higher (39.1%) ends of the [0–255] image intensity range. On average, 11% (28 levels) and up to 57% (149 levels) of the available intensity range were estimated to be underutilised. A substantial 72% of the cases demonstrating $th_l>0$ occurred on the top two subsectors of the field of view, whereas 70% of the cases demonstrating $th_t<255$ occurred on the bottom two subsectors. This observation suggests that signals at low-depth regions tend to be overamplified, whereas signals at larger depths are underamplified. This behaviour

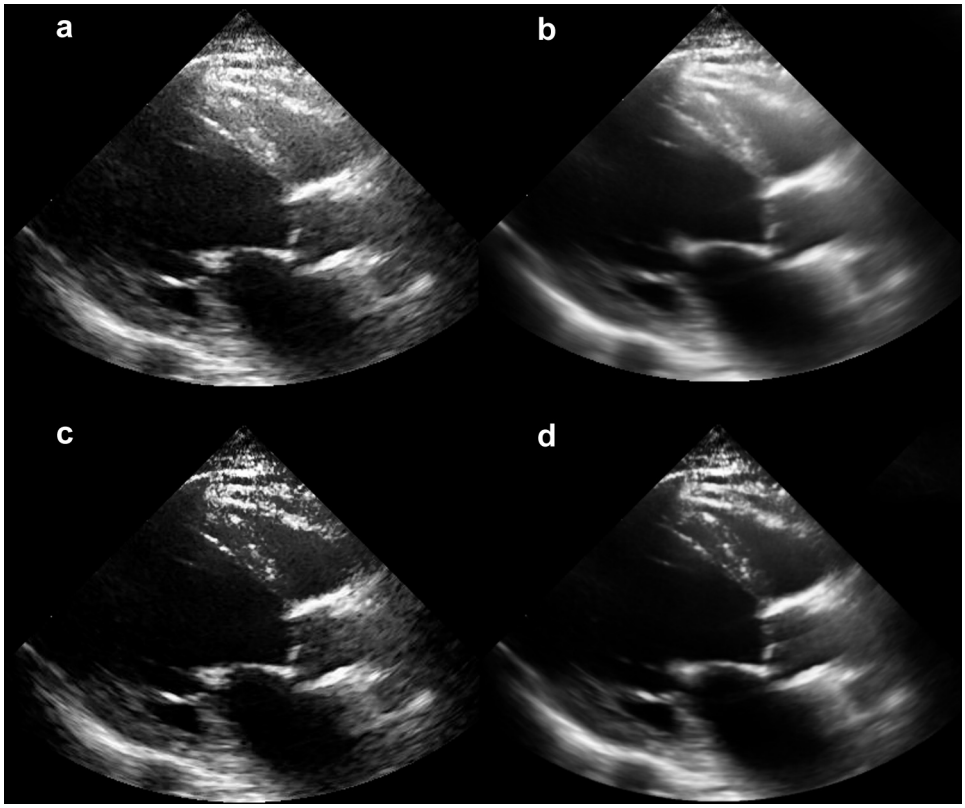

Fig. 8. Images characterised as of average diagnostic value. (a) Original, (b) compounded, (c) contrast-enhanced and (d) combined end-diastole frames.

can be partially attributed to non-optimal TGC manually set during data acquisition. Identifying and compensating for such underutilised intensity levels can provide a partial, indirect solution to the problem. Moreover, it provides a simple process increasing the dynamic range in the imaged structure for a more robust subsequent tissue/chamber identification.

Effect on SNR, contrast and SDNR

As outlined in Table 3, temporal compounding suppressed speckle and noise, increasing the average tissue (87.1%) and chamber (143.1%) SNR, as well as the associated tissue/chamber detectability (128.6%). On the other hand, temporal compounding had a negligible effect on tissue/chamber contrast. The proposed DHBIM enabled a large mean increase in contrast (73.8%) and detectability (120.9%) between cardiac tissue and chambers. The drop observed in the estimated SNRs should not necessarily be associated with increase in the noise within the signal. The tissue SNR increase is mostly generated by enhancing the underlying speckle patterns, providing valuable (*e.g.,* in speckle tracking applications) information on the imaged structure and relevant motion patterns. On the contrary, the chamber SNR is mostly noise, and its suppression is always desirable. However, spurious high-intensity noise in cardiac chambers can sometimes be misclassified (Fig. 5a,b,e) and enhanced as tissue, but. as illustrated in Figures 6 to 10, without any noticeable detrimental effect in the processed images. Simple morphologic filtering in the binary mask before the intensity mapping can also partially compensate for such spurious pixels. Finally, the integrated approach, combining contrast enhancement and temporal compounding, provides the only method improving all four image quality metrics, yielding a large mean increase in chamber SNR (78.2%) and tissue/chamber contrast (72.1%), as well as an impressive mean increase of 401.4% in tissue/chamber detectability (SDNR).

Visual effect

Figures 6 to 10 provide characteristic examples of the effects of each enhancement approach on clinical data (12 consecutive cardiac cycles) over a range of image quality and diagnostic value. Visual examination of the 32 data sets suggests that temporal compounding, as suggested by the relevant SNR increases (Table 3), can significantly reduce tissue speckle as well as noise in cardiac tissue and chambers. Furthermore, it can also enhance structures whose boundaries are hard to delineate because of high levels of noise or shadowing, such

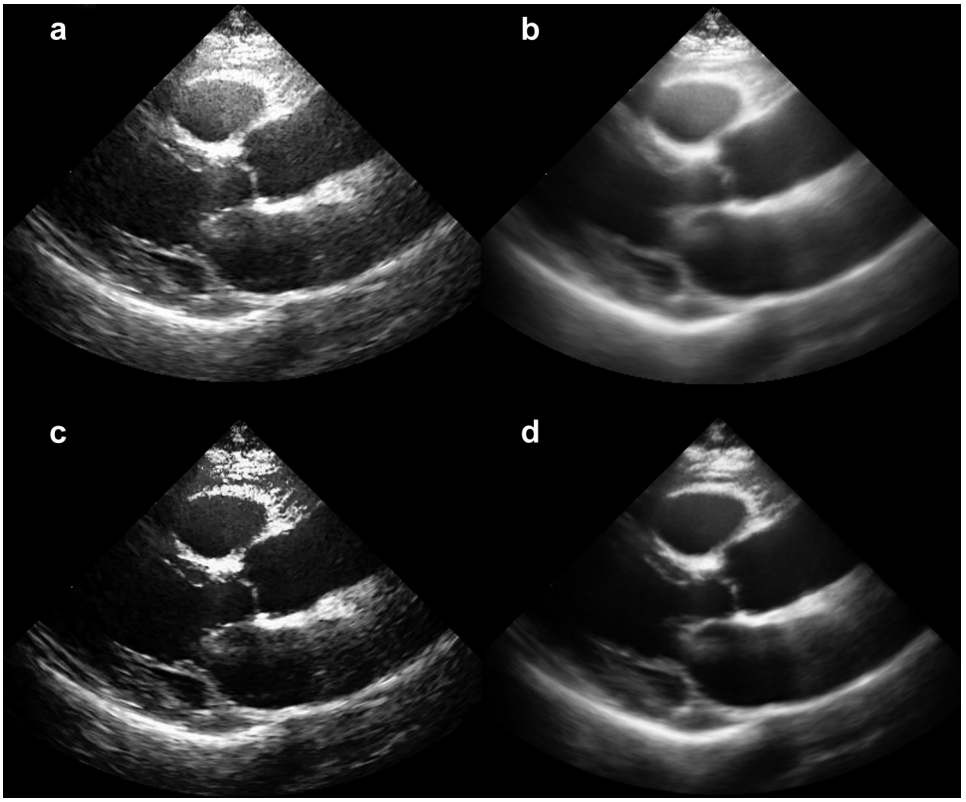

Fig. 9. Images characterised as of average diagnostic value. (a) Original, (b) compounded, (c) contrast-enhanced and (d) combined end-diastole frames.

as the RV and IVS (Figs. 8 and 10), the LVPW (Fig. 7) and the aortic valve in (Fig. 8). In Figure 6 is an example of very limited diagnostic value; although the quality of the data set remained low, structures such as the RV chamber and the LVPW were marginally enhanced, making them easier to delineate. On the other hand, temporal compounding has no noteworthy effect on tissue/chamber contrast and may introduce modest tissue/chamber boundary blurring, mostly around rapidly moving structures, such as valves (mitral valve in Figs. 8–10).

Visual examination of 32 data sets indicated that DHBIM can (i) generate a representative binary cardiac tissue mask (Fig. 5), (ii) suppress the cardiac chamber noise levels and (iii) increase the delineation of cardiac tissue. In general, the lower the image corruption levels are, the more representative the binary mask is. However, even in highly corrupted cases, the underlying tissue structure is fairly delineated (Figs. 5a and 6). Noticeable noise suppression occurs in the top half of the RV chamber, typically corrupted by near-field static noise (Figs. 6–10). Applying the algorithm in four non-overlapping sectors partially compensated for the variations in mean intensity and noise level among cardiac structures. A limitation of DHBIM occurs when high levels of noise, along with artifacts such as shadowing, mask out certain cardiac structures (IVS in Fig. 8). In such cases, the algorithm can misclassify and suppress the relevant pixel intensities of the corrupted tissue. Nevertheless, DHBIM has not been observed to suppress vital clinical information that is present in the original data set.

As illustrated in Figures 6 to 10, the integrated image enhancement method benefits from the advantages, whereas it compensates for the limitations of each individual method. In the first instance, the chamber noise is suppressed and the tissue/chamber contrast and detectability are enhanced, making cardiac structures clearly distinguishable. Likewise, tissue speckle as well as acoustic noise is further suppressed through spatial averaging. Averaging of spatiotemporally aligned frames also compensates for tissue structures that are heavily corrupted by noise or shadowing, which are otherwise misclassified and suppressed as chamber noise (aortic valve in Fig. 7, IVS in Fig. 8) by DHBIM. Furthermore, suppressing chamber noise and enhancing tissue/chamber contrast before image alignment result in a moderate reduction to the boundary blurring introduced during spatial compounding (mitral valve in Figs. 8 and 10). Nevertheless, low blurring levels are still observed, mostly around fast moving structures, such as valves, with some blurring identified along

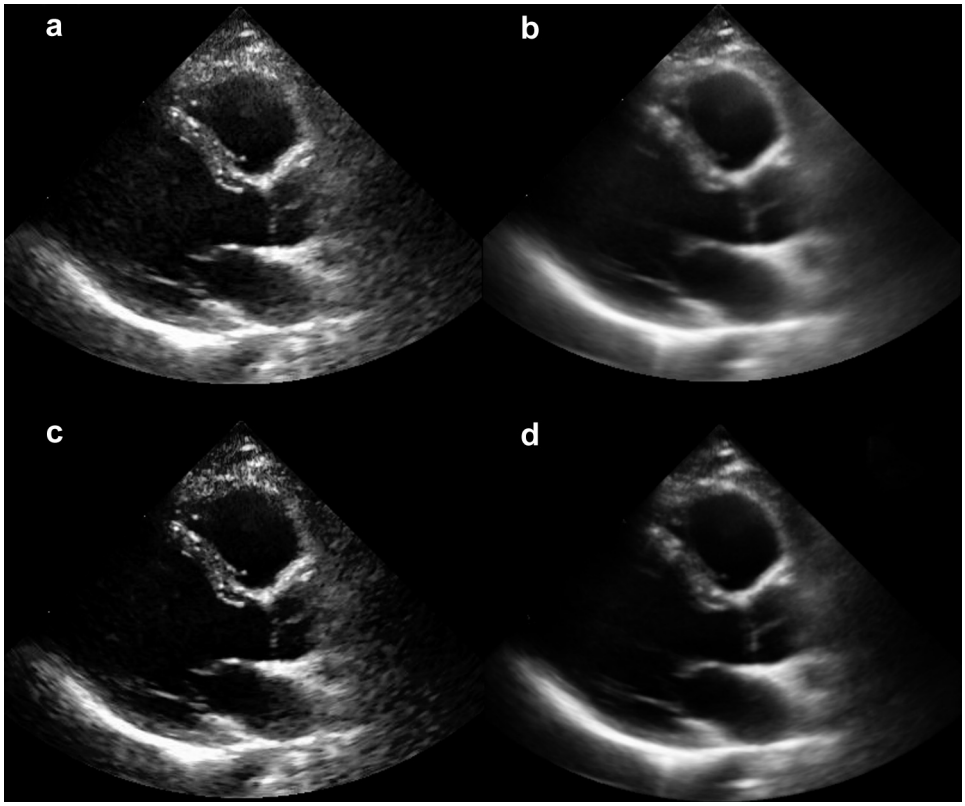

Fig. 10. Images characterised as of high diagnostic value. (a) Original, (b) compounded, (c) contrast-enhanced and (d) combined end-diastole frames.

chamber walls. The blurring effect is partially due to quantification errors as a result of the limited acquisition frame rate. Cardiac ultrasound scanners can acquire B-mode sequences at frame rates ≥100 Hz. Such an increase in temporal resolution (currently 25 Hz) is expected to further decrease the level of the tissue/chamber boundary blurring introduced.

Effect on diagnostic value

The repeatability and agreement plots derived for each of the five clinical measurements revealed (i) no major outliers and (ii) no substantial or systematic bias within each method or among the original and processed data. Furthermore, as suggested by Tables 4 and 5, the measurement agreement of each enhancement approach with the original measurement is on the same scale as the relevant measurement repeatability levels. Consequently, the results indicate a strong potential for the original and processed data to be interchangeable when performing cardiac measurements, and act as an additional aid in the diagnostic process, especially in challenging cases with corrupted imaged structures. In

Table 4. Comparison of effects of the individual and integrated image enhancement methods on clinical measurement repeatability

	Original		Compounded		Contrast enhanced		Integrated	
	Bias	Repeatability	Bias	Repeatability	Bias	Repeatability	Bias	Repeatability
IVSd	1.12	3.31	0.54	2.93	−0.30	3.49	0.27	2.87
LVIDd	−1.06	7.06	−0.25	4.73	0.47	6.12	−1.38	6.48
LVPWd	0.35	2.99	1.11	2.49	1.01	4.97	0.69	4.32
LADs	−0.31	4.17	0.27	5.64	0.11	4.68	−0.06	3.94
LVIDs	2.82	8.75	1.67	6.23	−1.06	5.22	0.47	3.77
Combined	0.52	6.22	0.64	4.80	0.07	5.16	−0.02	4.71

IVSd = end-diastole interventricular septal thickness; LVIDd = end-diastole left ventricular internal dimension; LVPWd = end-diastole left ventricular posterior wall; LADs = end-systole left atrium dimension; LVIDs = end-systole left ventricular internal dimension.

Table 5. Agreement of clinical measurements performed on processed images compared with measurements on original data

	Compounded		Contrast enhanced		Integrated	
	Bias	Agreement	Bias	Agreement	Bias	Agreement
IVSd	−0.36	3.63	−1.18	2.98	−1.00	3.62
LVIDd	0.19	7.17	0.60	5.73	−0.02	7.24
LVPWd	−0.24	3.37	−0.72	3.24	−0.45	3.51
LADs	0.48	3.94	−1.52	3.12	−1.18	2.72
LVIDs	−0.57	5.13	−1.28	5.03	−1.81	6.16
Combined	−0.08	4.92	−0.81	4.43	−0.87	5.09

IVSd = end-diastole interventricular septal thickness; LVIDd = end-diastole left ventricular internal dimension; LVPWd = end-diastole left ventricular posterior wall; LADs = end-systole left atrium dimension; LVIDs = end-systole left ventricular internal dimension.

particular, all three approaches improved the repeatability of the clinical measurements, with the integrated approach achieving the highest overall improvement of 24% (and highest improvement in three of the five measurements). On the other hand, DHBIM contrast enhancement achieved the lowest overall improvement with a reduction of the repeatability in two of the five measurements (LVPW and LAD). This reduction is potentially a result of the inability of DHBIM to compensate for heavily corrupted tissue structures that are therefore misclassified and suppressed as chamber noise. However, as suggested by their visual effect on cardiac images and indicated by the associated increase in LVPW and LAD measurement repeatability (13% and 16% respectively), the integrated approach can compensate for this limitation. Clinical measurement repeatability is expected to improve as the familiarity of the echocardiographer with the processed images increases. Given no observed degradation of high-quality images, the proposed integrated method has the potential to replace or act as an adjunct to existing image processing and display methods in ultrasonic scanners.

Limitations and future work

There are a number of limitations that, although beyond the scope of this work, will need to be addressed in future studies. In particular, the proposed algorithms can be further improved by making temporal compounding a fully automated approach. Currently, a single pair of ED and ES frames need to be manually identified by the clinician. The remaining ED and ES frames are then automatically identified using image similarity measures. Additional information, such as ECG data, LV shape/size parameters and tissue movement direction, can be incorporated to automatically classify all ED and ES frames. Furthermore, the current implementations of the proposed algorithms were aimed at the off-line processing and enhancement of cardiac ultrasound images. However, the real-time aspect of cardiac ultrasound constitutes a major advantage over other imaging modalities. Implementing the algorithms for the real-time or near real-time enhancement of cardiac ultrasound images can be of great benefit to the diagnostic process. Finally, the proposed algorithms have been thoroughly evaluated, on both image quality metrics as well as routine clinical measurements. However, a more extensive clinical assessment of the algorithms, including (i) direct comparison (on the same data) with other state-of-the-art enhancement approaches, (ii) on a wider range of imaging views (in addition to PLAX), and (iii) with a larger number of assessing expert echocardiographers will be of great value. Any subsequent study needs to ensure that images are acquired using a state-of-the-art device with optimal acquisition parameters such as axial, lateral and temporal resolution.

CONCLUSIONS

This study introduced DHBIM, a novel approach that employs variations of the cumulative histograms over time to estimate an intensity threshold between cardiac tissue and chambers and subsequently enhance their respective contrast. DHBIM reduces noise in cardiac chambers and improves the tissue/chamber contrast and detectability levels considerably. However, DHBIM does not compensate for tissue speckle and other common cardiac ultrasound artefacts such as shadowing and reverberations. Furthermore, there are cases in which heavily corrupted cardiac tissue structures are misclassified and suppressed as noise. Combining DHBIM with a temporal compounding to an integrated methodology can compensate for many of their individual limitations generating low-noise and high-contrast images with well-delineated cardiac structures. Assessment of the effect of each of the approaches on the image quality and diagnostic value of cardiac ultrasound data verified that although all three approaches can enhance the processed images, the integrated approach provided the best overall improvement.

Acknowledgments—This work was supported by the Engineering and Physical Sciences Research Council (EPSRC) through a Biologically Inspired Acoustic Systems grant (EP/C523776/1).

REFERENCES

Abdullah-Al-Wadud M, Kabir H, Dewan MAA, Chae O. A dynamic histogram equalization for image contrast enhancement. IEEE Trans Consumer Electronics 2007;53:593–600.

Abiko Y, Ito T, Nakajima M. Improvement on quality of echocardiograms. Acoust Imag 1997;23:169–176.

Achmad B, Mustafa MM, Hussain A. Inter-frame enhancement of ultrasound images using optical flow. Lecture Notes Comput Sci 2009; 5857:191–201.

Amorim JC, dos Reis M, de Carvalho JLA, da Rocha AF, Camapum JF. Improved segmentation of echocardiographic images using fusion of images from different cardiac cycles. In: Proceedings, IEEE Engineering in Medicine and Biology Society Conference, Minneapolis, Minnesota, USA. New York: IEEE; 2009. p. 511–514.

Averkiou MA, Roundhill DN, Powers JE. A new imaging technique based on the nonlinear properties of tissues. Proc IEEE Int Ultrason Symp 1997;1561–1566.

Barsky BA. End conditions and boundary conditions for uniform B-spline curve and surface representations. Comput Industry 1982;3: 17–29.

Becher H, Tiemann K, Schlosser T, Pohl C, Nanda NC, Averkiou MA, Powers JE, Luderitcz B. Improvement in endocardial border delineation using tissue harmonic imaging. Echocardiography 1998;15: 511–517.

Berne RM, Levy MN, Koeppen BM, Stanton BA. Physiology. St. Louis, MO: Elsevier; 2004.

Bland MJ, Altman DG. Statistical methods for assessing agreement between two methods of clinical measurement. Lancet 1986;327: 307–310.

Bray JJ, Cragg PA, Macknight ADC, Mills RG. Lecture notes on human physiology. Oxford: Blackwell Science; 1999.

Caglar H, Caglar N, Elfaituri K. B-Spline interpolation compared with finite difference, finite element and finite volume methods which applied to two-point boundary value problems. Appl Math Comput 2006;175:72–79.

Caidahl K, Kazzam E, Lidberg J, Neumann-Andersen G, Nordanstig J, Dahlqvist SR, Waldenstrom A, Wikh R. New concept in echocardiography: Harmonic imaging of tissue without use of contrast agent. Lancet 1998;352:1264–1270.

Department of Health Research and Development Directorate of England, National Institute for Social Care and Health Research of Wales, Chief Scientist Office of Scotland, R&D Division Public Health Agency of Northern Ireland. Governance arrangements for research ethics committees: A harmonised edition. London: Department of Health; 2011.

dos Reis M, Carvalho JLA, Macchiavello BL, Vasconcelos DF, da Rocha AF, Nascimento FAO, Camapum JF. On the use of motion-based frame rejection in temporal averaging denoising for segmentation of echocardiographic image sequences. In: Proceedings, IEEE Engineering in Medicine and Biology Society Conference. New York: IEEE; 2009. p. 507–510.

Feigenbaum H, Armstrong WF, Ryan T. Feigenbaum's echocardiography. Philadelphia: Lippincott Williams & Wilkins; 2005.

Finn S, Glavin M, Jones E. Echocardiographic speckle reduction comparison. IEEE Trans Ultrason Ferroelectr Freq Control 2011;58: 82–101.

Franke A, Hoffmann R, Kühl HP, Lepper W, Breithardt OA, Schormann M, Hanrath P. Non-contrast second harmonic imaging improves interobserver agreement and accuracy of dobutamine stress echocardiography in patients with impaired image quality. Heart 2000;83:133–140.

Fuster V, O'Rourke RA, Walsh RA, Poole-Wilson P. Hurst's the heart. New York: McGraw-Hill; 2008.

Gonzalez RC, Woods RE. Digital image processing. Engelwood Cliffs, NJ: Prentice Hall; 2001.

Gooding MJ, Rajpoot K, Mitchell S, Chamberlain P, Kennedy SH, Noble JA. Investigation into the fusion of multiple 4-D fetal echocardiography images to improve image quality. Ultrasound Med Biol 2010;36:957–966.

Guyton AC. Textbook of medical physiology. Philadelphia: Saunders; 1991.

Guyton AC, Hall JE. Human physiology and mechanisms of disease. Philadelphia: Saunders; 1997.

Hammoude A. Endocardial border identification in two-dimensional echocardiographic images: review of methods. Comput Med Imaging Graphics 1998;22:181–193.

Henry WL, DeMaria A, Gramiak R, King DL, Kisslo JA, Popp RL, Sahn DJ, Schiller NB, Tajik A, Teichholz LE, Weyman AE. Report of the American Society of Echocardiography Committee on Nomenclature and Standards in Two-Dimensional Echocardiography. Circulation 1980;62:212–217.

Ibrahim H, Kong NSP. Brightness preserving dynamic histogram equalization for image contrast enhancement. IEEE Trans Consumer Electronics 2007;53:1752–1758.

Klingler JW, Begeman MS, Fraker TD Jr, Andrews LT. Automatic detection of inter-frame motion in echocardiographic images. Ultrasound Med Biol 1989;15:683–689.

Li W, Gussenhoven EJ, Zhong Y, The SHK, Pieterman H, van Urk H, Bom K. Temporal averaging for quantification of lumen dimensions in intravascular ultrasound images. Ultrasound Med Biol 1994;20: 117–122.

Mulder HW, van Stralen M, van der Zwaan H, Leung KYE, Bosch JG, Pluim JPW. Multiframe registration of real-time three-dimensional echocardiography time series. J Med Imaging 2014;1:014004.

Nelder JA, Mead R. A simplex :method for function minimization. Comput J 1965;7:308–313.

Olstad B. ECG gated ultrasonic image compounding. U.S Patent 6447450 B1. GE Medical Systems Global Technology; 2002;. p. 16.

Perperidis A. Postprocessing approaches for the improvement of cardiac ultrasound B-mode images: A review. IEEE Trans Ultrason Ferroelectr Freq Control 2016;63:470–485.

Perperidis A, Cusack D, McDicken N, MacGillivray T, Anderson T. Temporal compounding of cardiac ultrasound data: Improving image quality and clinical measurement repeatability. In: Proceedings, IEEE Engineering in Medicine and Biology Society conference, 2009. Minneapolis, Minnesota, USA. New York: IEEE; 2009. p. 3661–3664.

Perperidis A, Cusack D, White A, McDicken N, MacGillivray T, Anderson T. Temporal compounding: A novel implementation and its impact on quality and diagnostic value in echocardiography. Ultrasound Med Biol 2015;41:1749–1765.

Petrovic O, Feigenbaum H, Armstrong WF, Ryan T, West SR, Creen-Hess D, Stewart J, Friedmeyer JL, Fineberg NS. Digital averaging to facilitate two-dimensional echocardiographic measurements. J Clin Ultrasound 1986;14:367–372.

Rajpoot K, Noble JA, Grau V, Szmigielski C, Becher H. Multiview RT3D echocardiography image fusion. Lecture Notes Comput Sci 2009;5528:134–143.

Rajpoot K, Grau V, Noble JA, Szmigielski C, Becher H. Multiview fusion 3-D echocardiography: Improving the information and quality of real-time 3-D echocardiography. Ultrasound Med Biol 2011; 37:1056–1072.

Rigney DR, Wei JY. A novel motion detection method for improving the quality of two-dimensional echocardiographic images. J Am Soc Echocardiogr 1988;1:127–134.

Sezgin M, Sankur B. Survey over image thresholding techniques and quantitative performance evaluation. J Electronic Imaging 2004; 13:146–168.

Szmigielski C, Rajpoot K, Grau V, Myerson SG, Holloway C, Noble JA, Kerber R, Becher H. Real-Time 3 D Fusion Echocardiography. JACC Cardiovasc Imaging 2010;3:682–690.

Tay PC, Garson CD, Acton ST, Hossack JA. Ultrasound despeckling for contrast enhancement. IEEE Trans Image Process 2010;19: 1847–1860.

Unser MA, Dong L, Pelle G, Brun P, Eden M. Restoration of echocardiograms using time warping and periodic averaging on a normalized time scale. SPIE Proc Med Imaging 1989;84–93.

van Ocken E, Glaes VA, Brutsaert DL. Image enhancement by digital averaging of 2-dimensional echopictures. In: Proceedings, Fourth European Congress on Ultrasound in Medicine, Amsterdam, The Netherlands. Amsterdam: Elsevier/North-Holland; 1981. p. 69.

Vitale DF, Lauria G, Pelaggi N, Gerundo G, Bordini C, Leosco D, Rengo C, Rengo F. Optimal number of averaged frames for noise

reduction of ultrasound images, Proceedings, IEEE Computers in Cardiology Conference, London, UK. New York: IEEE; 1993. p. 639–641.

Ward B, Baker AC, Humphrey VF. Nonlinear propagation applied to the improvement of resolution in diagnostic medical ultrasound. J Acoust Soc Am 1997;101:143–154.

Wharton G, Steeds R, Allen J, Brewerton H, Jones R, Kanagala P, Lloyd G, Masanim N, Mathew T, Oxborough D, Rana B, Sandoval J, Smith N, Wheele R. A minimum dataset for a standard transthoracic echocardiogram. London: British Society of Echocardiography; 2012. p. 1–6.

Yao C, Penney GP. Spatial compounding of 3-D echocardiography: Novel methodologies for large sets of images. In: Proceedings, Medical Image Understanding and Analysis Conference. The British Machine Vision Association and Society for Pattern Recognition; Dundee, UK. 2008.

Yao C, Simpson JM, Schaeffter T, Penney GP. Spatial compounding of large numbers of multi-view 3 D echocardiography images using feature consistency. In: Proceedings, IEEE International Symposium in Biomedical Imaging: From Nano to Macro, London, UK, SPIE Proc 2010;7265:968–971.

Yue Y, Croitoru MM, Bidani A, Zwischenberger JB, Clark JW. Ultrasound speckle suppression and edge enhancement using multiscale nonlinear wavelet diffusion. In: Proceedings, IEEE Engineering in Medicine and Biology Conference. New York: IEEE; 2005.

Zong X, Laine AF, Geiser EA. Speckle reduction and contrast enhancement of echocardiograms via multiscale nonlinear processing. IEEE Trans Med Imaging 1998;17:532–540.

Zwirn G, Akselrod S. A histogram-based technique for echocardiographic image enhancement. Proc Comput Cardiol Conf 2004;81–84.

Zwirn G, Akselrod S. Adaptive brightness transfer functions in echocardiography. Ultrasound Med Biol 2005;31:649–661.